JOURNAL OF Applied Polymer SCIENCE

Crystallization Behavior of Ultrahigh-Molecular-Weight Polyethylene/Polyhedral Oligomeric Silsesquioxane Nanocomposites Prepared by Ethylene *In Situ* Polymerization

Chao Guan,[1] Huaqin Yang,[1] Wei Li,[1,2] Danying Zhou,[1] Jie Xu,[1] Zhong-Ren Chen[1,2]

[1]Department of Polymer Science and Engineering, Faculty of Materials Science and Chemical Engineering, Ningbo University, Ningbo 315211, People's Republic of China

[2]Key Laboratory of Specialty Polymers, Grubbs Institute, Ningbo University, Ningbo 315211, People's Republic of China

Correspondence to: W. Li (E-mail: liwei@nbu.edu.cn) and Z.-R. Chen (E-mail: chenzhongren@nbu.edu.cn)

ABSTRACT: A [3-*t*-Bu-2-O—C_6H_3CH═N(C_6F_5)]$_2$TiCl_2 catalyst (bis(phenoxyimine)titanium dichloride complex - FI catalyst) was immobilized on disilanolisobutyl polyhedral oligomeric silsesquioxane (OH-POSS) to prepare ultrahigh molecular-weight polyethylene (UHMWPE)/polyhedral oligomeric silsesquioxane (POSS) nanocomposites during ethylene *in situ* polymerization. The dispersion state of POSS in the UHMWPE matrix was characterized by X-ray diffraction measurements and transmission electron microscopy. It was shown that the OH-POSS achieved uniformed dispersion in the UHMWPE matrix, although its polarity was unmatched. The isothermal and nonisothermal crystallization behavior of the nanocomposites was investigated by means of differential scanning calorimetry. The crystallization rate of the nanocomposites was enhanced because of the incorporation of POSS during the isothermal crystallization. POSS acted as a nucleus for the initial nucleation and the subsequent growth of the crystallites. For nonisothermal studies, POSS showed an increase in the crystallinity. The crystallization rate of the nanocomposites decreased because the presence of POSS hindered the crystal growth. © 2014 Wiley Periodicals, Inc. J. Appl. Polym. Sci. **2014**, *131*, 40847.

KEYWORDS: crystallization; nonpolymeric materials and composites; polyolefins

Received 1 March 2014; accepted 8 April 2014
DOI: 10.1002/app.40847

INTRODUCTION

Ultrahigh-molecular-weight polyethylene (UHMWPE) is a kind of high-density polyethylene with its weight-average molecular weight (M_w) of up to 1,000,000 g/mol.[1] Because of the large numbers of entanglements and extremely long molecular chains, the mobility of the UHMWPE chains is very much limited; this results in an extremely high melt viscosity of the polymer.[2–4] Hence, UHMWPE is very difficult to process by conventional methods. Generally, the incorporation of a small amount of inorganic nanofillers into the polymer matrix can endow the polymer with new and much improved mechanical, thermal, and electrical properties.[5,6] However, UHMWPE nanocomposites are always synthesized by solvent-blending methods because of their worse processability. Fang et al.[7] synthesized a hydroxyapatite (HA) particulate reinforced UHMWPE nanocomposite by compounding HA and UHMWPE mixtures in paraffin oil using twin-screw extrusion and then compression molding. Nanosized HA in the matrix of UHMWPE could be used as a biocomposite thanks to the biocompatibility of polyethylene coupled with the osseointegration capabilities of HA. Rastogi et al.[8] developed a new method for preparing UHMWPE/single-walled carbon nanotube (SWCNT) nanocomposites on the basis of solution-blending methods. The dispersion was obtained by the spraying of an aqueous solution of SWCNTs onto a fine UHMWPE powder directly obtained from synthesis. The SWCNTs were adsorbed on the surface of the polymer powder. A composite film was prepared from the solution of the polymer powder dissolved in xylene. The high viscosity of UHMWPE prevented coagulation of the adsorbed SWCNTs.

The synthesis of good performance in the polymer nanocomposites and the hindrance of the formation of nanofiller aggregators is very important, especially when the polarity of the filler is unmatched with the matrix.[9] To overcome the van der Waal's bonding of nanofillers to achieve exfoliation of the filler, the *in situ* polymerization approach has been developed.[10] The catalyst for ethylene polymerization is introduced into a gallery of the filler, after which polyethylene forms *in situ*, and the aggregation morphology delaminates.[11] This method is efficient in the preparation of exfoliated nanocomposites because the entropy

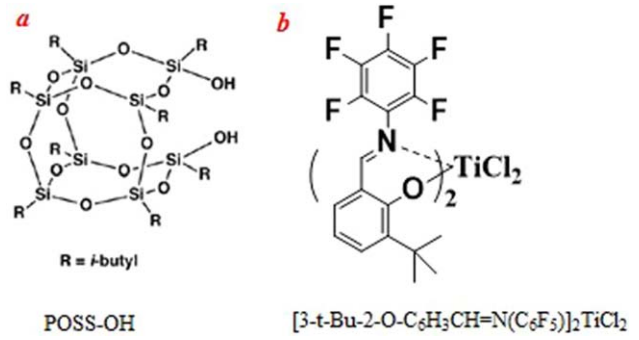

Figure 1. Molecular structures of the (a) POSS and (b) FI catalyst used in this study. [Color figure can be viewed in the online issue, which is available at wileyonlinelibrary.com.]

resistance for the intercalation of polymer chains significantly decreases, and the heat released by polymerization acts favorably to reduce the process-free energy.[12]

It is worth noting that fillers can either promote or retard the crystallization of the polymers; this depends on the dispersion and loading content of the fillers in thermoplastic matrices.[13,14] Ahangari et al.[13] showed the isothermal and nonisothermal crystallization behaviors of the neat isotactic polypropylene (iPP) and melt-blended iPP/SWCNTs nanocomposites containing 0.5 wt % SWCNTs. The addition of a nucleating agent into the polymer matrix increases the crystallization rate (ϕ) and decreases the crystallization half-time of iPP remarkably. Shi et al.[14] studied the influence of the nanofiller dimensionality on the crystallization behavior of HDPE/carbon nanocomposites. They observed that carbon nanofillers with different dimensionalities affected the crystal growth mechanism. In this study, disilanolisobutyl polyhedral oligomeric silsesquioxane (OH-POSS) was used to combine the [3-*t*-Bu-2-O-C_6H_3CH-N(C_6F_5)]$_2TiCl_2$ catalyst (bis(phenoxyimine)titanium dichloride complex - FI catalyst) to prepare UHMWPE/polyhedral oligomeric silsesquioxane (POSS) nanocomposites by ethylene *in situ* polymerization. It was the first time that the influence of the polarity of POSS on the crystallization kinetics of UHMWPE were examined.

EXPERIMENTAL

Materials

The [3-*t*-Bu-2-O-C_6H_3CH-N(C_6F_5)]$_2TiCl_2$ (FI catalyst) used in the investigation was synthesized according to the literature.[15,16] OH-POSS was purchased from Hybrid Co. and dried for 24 h before use. Figure 1 depicts the structure of the FI catalyst and the OH-POSS. Polymerization-grade ethylene and nitrogen were purchased from Fangxin Ningbo Corp. (Ningbo, China) and were purified by filtration through Mn molecular sieves and subsequent 5-Å molecular sieves. Methylaluminoxane (10 wt % solution in toluene) was purchased from Albermarle Chemical, Inc. Toluene (Ningbo Chemical Reagents Co., China) were purified over sodium/benzophenone ketyl and distilled before use. All manipulations were made with Schlenk techniques or a glovebox.

Preparation of the POSS Combined FI Catalyst (FI/POSS Catalyst)

Amounts of 500 mg of POSS and 83.6 mg of the FI catalyst were dissolved in 50 mL of toluene for 1 h, respectively. The molar ratio of -OH (POSS) to -Cl (FI catalyst) was maintained at 4.0. After that, the FI catalyst solution was added to the POSS solution drop by drop. The mixture was stirred for 24 h at room temperature in the glovebox to obtain a totally transparent homogeneous catalyst solution, which was termed the FI/POSS catalyst.

Ethylene Polymerization

Ethylene polymerization was carried out in a 100-mL glass reactor equipped with a mechanical stirrer. The reactor temperature was set to 30°C. A volume of 50 mL of toluene was added to the reactor. An amount of 1 μmol of the catalyst was introduced into the reactor under nitrogen purging after the injection of appropriate methylaluminoxane as the cocatalyst. The polymerization then took place under a continuous ethylene flow to meet 1 bar at a stirring rate of 100 rpm. The concentration of POSS in the polymer matrix was modulated by the variation of the polymerization time. The obtained polymer was precipitated and washed with acidified (2 wt % hydrochloric acid) ethanol, filtered, and dried at 50°C *in vacuo* for 12 h.

Characterization and Analysis

Gel Permeation Chromatography (GPC) Measurements. The M_w and molecular weight distribution (MWD) were determined with GPC at 150°C with a PL-GPC-220 instrument (Polymer Laboratories, United Kingdom) with 1,2,5-trichlorobenzene as the solvent.

X-ray Diffraction (XRD) Measurements. XRD measurements were carried out on a Bruker GADDS diffractometer with an area detector operating under 40 kV and 40 mA with Cu Kα radiation ($\lambda = 0.154$ nm).

Transmission Electron Microscopy (TEM) Characterization. The morphology of the polymers was monitored by TEM (Tecnai F20).

Crystallization Study. Differential scanning calorimetry (DSC) was performed with a Hyper DSC 8500 instrument (PerkinElmer Corp.) to measure the melting point and crystallinity of polyethylene. The samples (ca. 8 mg) were first heated to 160°C at a rate of 10°C/min and then cooled to 50°C at the same rate. The second heating cycle was conducted at the same heating rate. The melting temperature (T_m) was taken at the peak of the endotherm. The crystallinity was calculated by comparison with the heat of fusion of a perfectly crystalline polyethylene, that is, 289 J/g.

An isothermal crystallization and nonisothermal crystallization study of the polymers was carried out under a nitrogen atmosphere with DSC. Samples of approximately 8 mg were used for each run. The samples were first heated from 30 to 160°C at a rate of 50°C/min and then held for 5 min. After that, the samples were rapidly cooled to the designated crystallization temperature ($T_c = 150$°C/min) and kept at that temperature until the crystallization was completed. To ensure the integrity of the isothermal crystallization process and the reliability of the calculated kinetic data, proper temperatures for isothermal crystallization were selected. For this reason, the isothermal crystallization measurements of each sample were carried out at in the temperature range 118–120°C.

To examine nonisothermal crystallization, the samples were heated from 30 to 180°C, held for 5 min, and then cooled to

Table I. Microstructures of the Polymers Obtained from the FI/POSS and FI Catalyst System[a]

Entry	Time (min)	POSS load (wt %)[b]	X_c^1 (%)	X_c^2 (%)	T_m^1 (°C)	T_m^2 (°C)	M_w (10^6 g/mol)	M_n (10^6 g/mol)	MWD
1[c]	10	0.0	65.8	25.2	142.2	134.8	1.17	0.76	1.54
2	40	1.0	71.3	27.1	143.3	135.4	1.68	0.39	4.33
3	30	1.5	74.1	29.5	143.3	135.9	1.36	0.42	3.23
4	20	2.3	74.9	31.2	143.6	136.4	1.28	0.47	2.73

M_n, number-average molecular weight.
[a] All reactions were performed in a 100-mL reactor at 30°C and 1 bar with 50 mL of toluene. X_c^1 is the crystallinity during the first heating scan, X_c^2 is the crystallinity during the second heating scan, T_m^1 is the melting point during the first heating scan, and T_m^2 is the melting point during the second heating scan.
[b] The load of POSS was determined by thermogravimetric analysis with a heating temperature ranging from 50 to 600°C at a heating rate of 10°C/min.
[c] Run 1 was performed with the FI catalyst; the other runs were performed with the FI/POSS catalyst.

30°C at constant cooling rates of 5, 10, 15, and 20°C/min. The absolute crystallinity of the polymer was determined by standard DSC scans. The samples were cooled from the melt (180°C) to 25°C at 10°C/min, held there for 5 min, and then heated to 180°C at 10°C/min.

RESULTS AND DISCUSSION

Preparation of the UHMWPE/POSS Nanocomposites

Table I lists the results of the polymerization and the polymer characterizations. All of the M_w values of the synthesized polyethylene were up to 1,000,000 g/mol. This suggested that UHMWPE and UHMWPE/POSS nanocomposites were obtained. Fortunately, the synthesized polymers had similar molecular weights. This was very important in the study of the crystallization behaviors. Interestingly, we found that the synthesized UHMWPE presented a high T_m (>141°C) during the first heating scans. Such a high T_m is normally found for chain-extended polyethylene crystals, which are extremely thick (>1 μm).[17] Furthermore, the high T_m of 141°C was lost in the second heating, where a T_m of 134°C was found. The melting point and the crystallinity obviously increased when the POSS loading increased. This indicated that POSS could be used as a nucleating agent[18] to enhance the crystalline behaviors of the nascent UHMWPE chains.

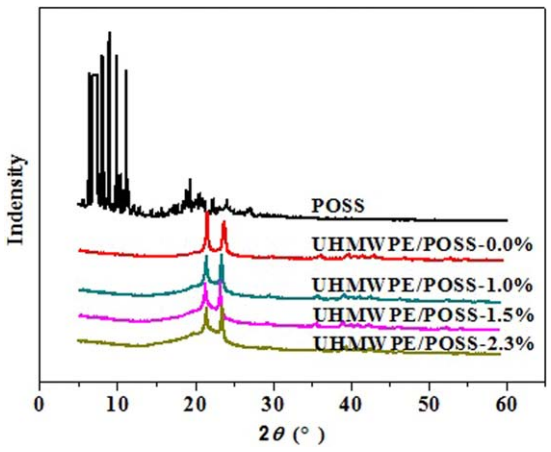

Figure 2. XRD patterns of the UHMWPE and UHMWPE/POSS nanocomposites. [Color figure can be viewed in the online issue, which is available at wileyonlinelibrary.com.]

Dispersion of POSS in the UHMWPE Matrix

A typical POSS cage consists of 8, 10, or 12 Si atoms with an Si/O ratio of 2:3, an Si-Si diameter of 0.54 nm, and an Si-C bond length in the range 1.83–2.03 Å. The eight organic corner groups can be functionalized with a variety of organic substituents.[19,20] With this unique structure, POSS molecules are widely used in the preparation of nanocomposites. OH-POSS is a kind of polar filler because of the Si-O-Si cage structure and hydroxyl groups. Generally, OH-POSS cannot achieve a homogeneous dispersion state in polyethylene matrix because of their unmatched solubility parameters. The OH-POSS always tends to aggregate during the physical blending process. Hence, the dispersion state of OH-POSS in the UHMWPE matrix was the fundamental information used to investigate the isothermal and nonisothermal crystallization.

Figure 2 shows the XRD patterns of the pure UHMWPE, POSS, and nanocomposites for 2θ values from 4 to 60°. For UHMWPE and its nanocomposites, two main reflections were observed at 2θ values of 21 and 24°; these were attributed to the 110 and 200 crystal planes, respectively. The polymer matrix did not have any peaks from 7 to 12°, where POSS had typical reflections in this region. This indicated that the crystalline structure of the POSS clusters was completely disrupted.[19,21,22]

Figure 3 shows the TEM images of the UHMWPE nanocomposites that had the highest POSS loading. OH-POSS was dispersed uniformly in the UHMWPE matrix with particles size of only several tens of nanometers. this suggested that the aggregation of

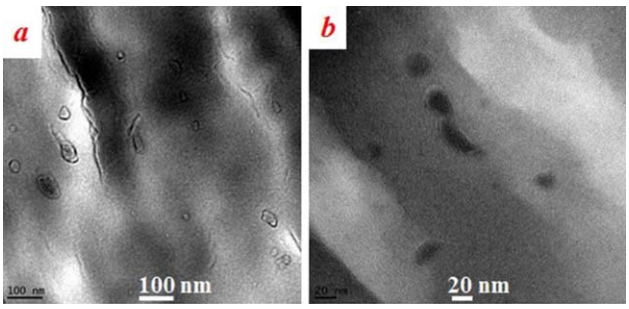

Figure 3. TEM images of the nascent UHMWPE/POSS-2.3% at different magnifications. [Color figure can be viewed in the online issue, which is available at wileyonlinelibrary.com.]

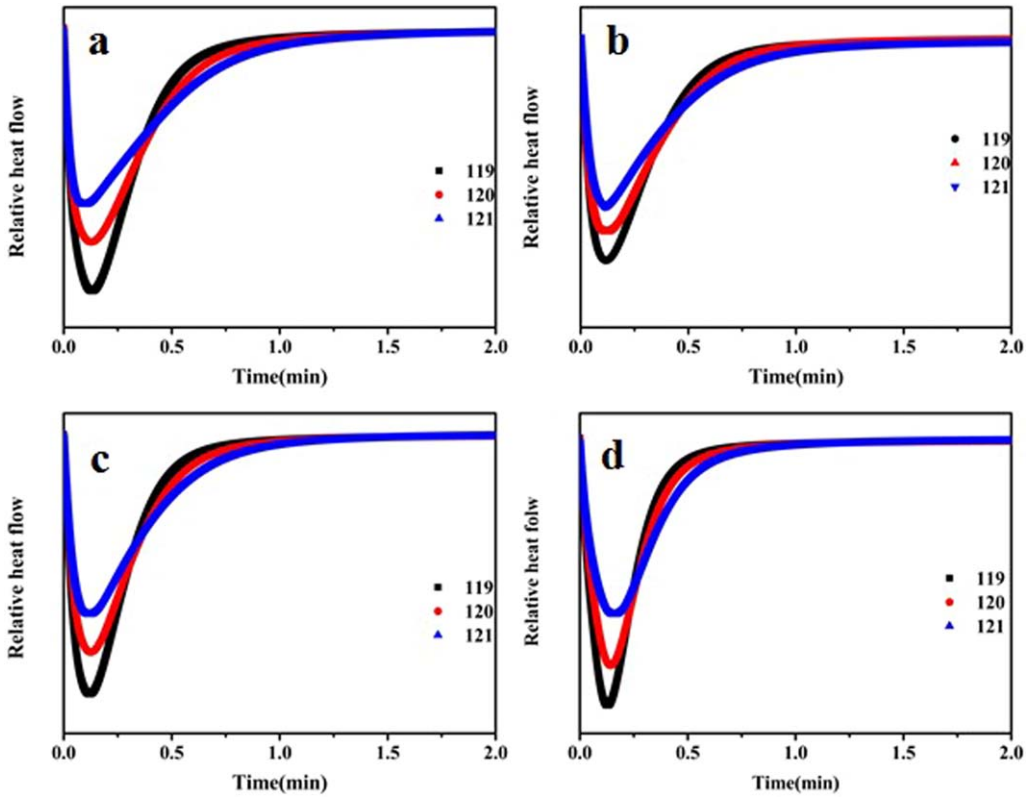

Figure 4. DSC curves of the isothermal crystallization of the UHMWPE and UHMWPE/POSS nanocomposites at different T_c's: (a) UHMWPE/POSS-0.0%, (b) UHMWPE/POSS-1.0%, (c) UHMWPE/POSS-1.5%, and (d) UHMWPE/POSS-2.3%. [Color figure can be viewed in the online issue, which is available at wileyonlinelibrary.com.]

POSS molecules was hindered. Only several POSS molecules could be contained in each POSS particle. This further proved the foundation of the XRD results. These observations presented a view of the *in situ* polymerization process with the FI/POSS catalyst. The UHMWPE chains grew from the active sites anchored on the POSS particles and then encapsulated the POSS particles to form the basic units of the nanocomposites. The hydraulic forces generated from chain growth and the heat released by polymerization acted favorably to overcome the van der Waal's bonds and the hydrogen bonds between the POSS molecules; this resulted in the uniform dispersion.

Isothermal Crystallization Analysis

The isothermal crystalline behaviors of the polymers were investigated to quantitatively study the crystalline ability of the polymer chains based on the Avarami and Tobin methods. Generally, the Avarami equation[23,24] is used to analyze the isothermal crystallization kinetics of polymers:

$$X_t = 1 - \exp\left[-(K_a t)^{n_a}\right] \tag{1}$$

where X_t is the relative crystallinity at time t, K_a is the Avrami crystallization rate constant, and n_a is the Avrami exponent, which reveals the nucleation mechanism. As Avarami analysis is appropriate for describing the early stages of polymer crystallization, Tobin theory,[25] which involves the phase-transformation kinetics with growth site impingement, was thus proposed to improve the fitting results in the later stages of crystallization:

$$X_t = \frac{(K_t t)^{n_t}}{1 + (k_t t)^{n_t}} \tag{2}$$

where K_t is the Tobin crystallization rate constant and n_t is the Tobin exponent governed by different types of nucleation and growth mechanisms.

Figure 4 shows the typical isothermal crystallization curves of polyethylene at different T_c's. The crystallization exothermic peaks became flatter with increasing T_c. Meanwhile, the time to complete crystallization was increased. X_t was obtained from the area under the exotherm up to time t divided by the total exothermic peak area:

$$X_t = \frac{\int_0^t \frac{dH_c}{dt}\,dt}{\int_0^\infty \frac{dH_c}{dt}\,dt} \tag{3}$$

where dH_c is the enthalpy of crystallization released during an infinitesimal time interval d_t. Thus, the development of X_t with the crystallization time for polyethylene was established (Figure 5).

Table II summarizes the fitting results of the isothermal crystallization. It is shown that the Tobin method had the best consistency between the data and the model because of its smallest derivation; this indicated that the chain-impinging effect could not be ignored during the crystallization.[26]

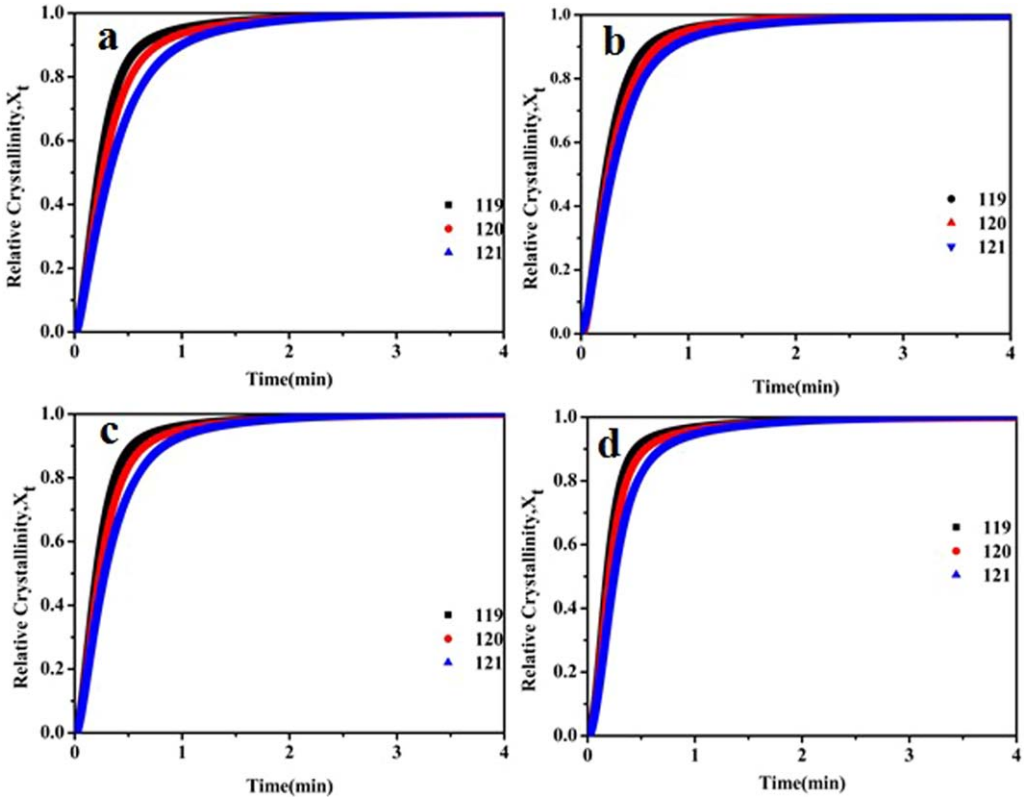

Figure 5. Development of X_t with the crystallization time for the isothermal crystallization of (a) UHMWPE/POSS-0.0%, (b) UHMWPE/POSS-1.0%, (c) UHMWPE/POSS-1.5%, and (c) UHMWPE/POSS-2.3%. [Color figure can be viewed in the online issue, which is available at wileyonlinelibrary.com.]

Generally, half time of crystallization ($t_{1/2}$) of a polymer is taken as a measure of the overall rate of crystallization. Table II shows that the $t_{1/2}$ of all of the polymers increased with increased T_c. This verified that the crystallization took place by a nucleation-controlled mechanism.[26,27] Furthermore, the values of n_a and n_t were approximately equal for all of the polymers. This indicated that the polymers had the same crystalline mechanism.[14] The values of n_t, generally approximately equal to n_a +1, also remained close to 2; this indicated the simultaneous occurrence of two-dimensional crystal growth with heterogeneous nucleation.[27] The crystallization rate constants k_α and k_t were also affected by the concentration of POSS, as we observed a pronounced increase in their values with increasing POSS content. It is possible that POSS acted as a nucleus for the initial nucleation and subsequent growth of the crystallites.

Table II. Kinetic Parameters of the Avrami and Tobin Models

		Avrami			Tobin			
	T_c (°C)	k_α (min^{-1})	n_α	R^2	k_t (min^{-1})	n_t	R^2	$t_{1/2}$
UHMWPE/POSS-0.0%	119	3.3294	1.2655	0.9951	4.6207	2.1236	0.9990	0.2250
	120	2.7254	1.1368	0.9934	3.8959	1.9397	0.9993	0.2630
	121	2.2254	1.0617	0.9962	3.2460	1.8472	0.9978	0.3160
UHMWPE/POSS-1.0%	119	3.2196	1.2402	0.9941	4.4999	2.0657	0.9994	0.2180
	120	2.8452	1.1949	0.9949	4.0163	2.0151	0.9991	0.2550
	121	2.4590	1.1340	0.9959	3.5235	1.9413	0.9985	0.2900
UHMWPE/POSS-1.5%	119	3.6693	1.2607	0.9922	5.1045	2.0824	0.9995	0.2010
	120	3.1183	1.1953	0.9926	4.4008	2.0059	0.9996	0.2320
	121	2.5867	1.1184	0.9948	3.7201	1.9192	0.9990	0.2740
UHMWPE/POSS-2.3%	119	4.2092	1.3763	0.9888	5.7219	2.2057	0.9988	0.1780
	120	3.6564	1.3147	0.9881	5.0274	2.1353	0.9990	0.2020
	121	2.9928	1.2332	0.9896	4.1824	2.0542	0.9996	0.2430

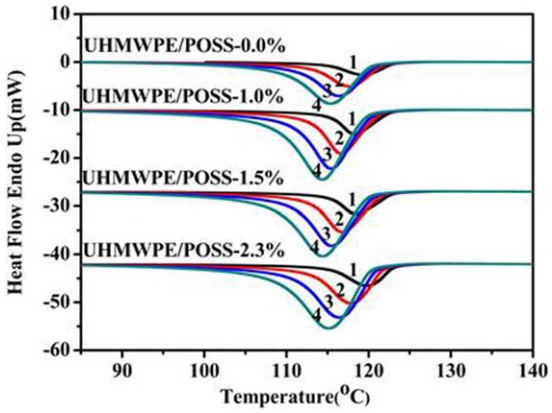

Figure 6. DSC curves of the nonisothermal crystallization of the UHMWPE/POSS nanocomposites at different cooling rates: (1) 5, (2) 10, (3) 15, and (4) 20°C/min. [Color figure can be viewed in the online issue, which is available at wileyonlinelibrary.com.]

Nonisothermal Crystallization Analysis

The nonisothermal melt crystallization exotherms for UHMWPE and its nanocomposites at different cooling rates are shown in Figure 6. As the cooling rate increased, the exothermic traces became wider and shifted to lower temperatures for all of the samples. In all cases, the peak crystallization temperature (T_p), which corresponded to the maximum ϕ, decreased with increasing cooling rate; this indicated that the crystallization process was controlled by the nucleation rate.[28] The lower cooling rate provided sufficient time for the polymer chains to align themselves. Figure 6 shows that the exothermic traces gradually broadened with the addition of POSS in the UHMWPE matrix. This may have been due to the increased MWD of the UHMWPE nanocomposites.

Table III lists the enthalpy of crystallization (ΔH_c) values determined from the DSC curves (Figure 7). For a given cooling rate, we observed that the incorporation of POSS in UHMWPE led to a successive increase in ΔH_c. The result was consistent with that of the isothermal crystallization studied previously. With the addition of POSS, the incubation time to reach the critical equilibrium nucleus dimension became shorter. Thus, the increased ΔH_c may have been due to the nucleating effect of the incorporated POSS.

The nonisothermal crystallization behavior was analyzed by both the Ozawa and Mo methods. The Ozawa plots of UHMWPE are shown in Figure 8 as an example. The Ozawa plots of all of the samples deviated from linear zoom at different cooling rates; this suggested that the Ozawa equation was not appropriate for describing the nonisothermal crystallization of these polymers. The Ozawa method ignores the secondary crystallization, whereas for a semicrystalline polymer such as polyethylene, a large portion of the crystallinity is attributed to the secondary crystallization.

The Mo model [eq. (4)] is hence used to analyze the nonisothermal crystallization of UHMWPE and its nanocomposites:

$$\log \phi = \log F(T) - B \log t \tag{4}$$

where the parameter $F(T)$ refers to the value of the cooling rate required to reach a certain degree of crystallinity at unit crystallization time and B is the ratio between the Avrami and Ozawa exponents. Thus, the plotting of log ϕ versus log t at a given X_t yields a linear relationship between log ϕ and log t. The values of B and $F(T)$ were estimated from the slope and the intercept of the line. The values are summarized in Table IV. The small variation in the value of B for each sample and the clear linear relation between log ϕ and log t (Figure 9) indicated that the Mo method was applicable for describing the nonisothermal behavior of the UHMWPE and

Table III. Nonisothermal Parameters of UHMWPE/POSS Determined from DSC Exotherms

Sample	Φ (°C/min)	T_{onset} (°C)	T_c (°C)	ΔH_c (J/g)
UHMWPE/POSS-0.0%	5	123.2	119.3	65.38
	10	122.0	117.7	69.85
	15	121.0	116.4	76.80
	20	120.2	115.4	76.89
UHMWPE/POSS-1.0%	5	122.5	118.3	73.41
	10	121.2	116.6	83.45
	15	120.3	115.4	90.32
	20	119.5	114.4	95.65
UHMWPE/POSS-1.5%	5	123.0	118.5	75.64
	10	121.6	116.8	88.43
	15	120.6	115.5	92.18
	20	119.8	114.4	94.36
UHMWPE/POSS-2.3%	5	123.2	119.7	76.96
	10	122.0	117.9	92.21
	15	121.1	116.4	95.45
	20	120.3	115.2	95.74

Φ = heating rate; T_{onset} = starting crystallization temperature.

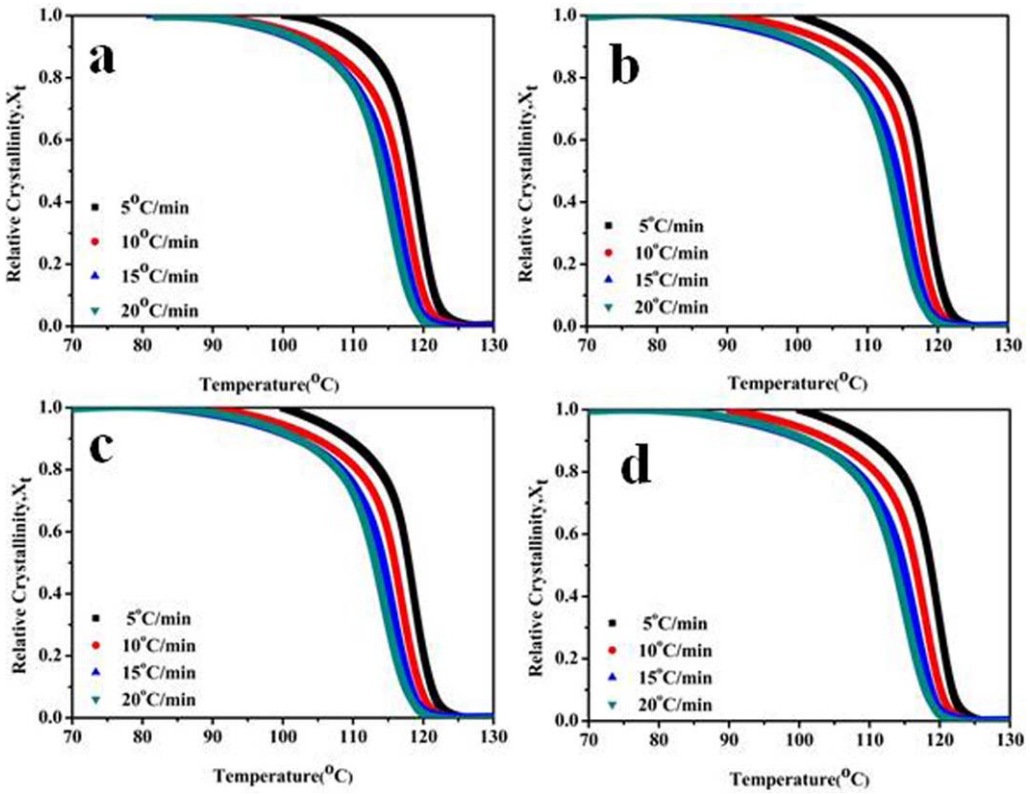

Figure 7. Development of X_t with the temperature for the nonisothermal crystallization of UHMWPE/POSS: (a) UHMWPE/POSS-0.0%, (b) UHMWPE/POSS-1.0%, (c) UHMWPE/POSS-1.5%, and (d) UHMWPE/POSS-2.3%. [Color figure can be viewed in the online issue, which is available at wileyonlinelibrary.com.]

UHMWPE/POSS nanocomposites. At a given X_t, the values of $F(T)$ increased when more POSS was incorporated into the UHMWPE matrix. The higher values of $F(T)$ showed that the corresponding nanocomposites could achieve the same degree of crystallinity, which was slower than the pure UHMWPE; this indicated a slowdown of ϕ. This seemed contrary to the results of the isothermal crystallization procedure, where ϕ increased. Generally, ϕ is controlled by the nucleation and crystal growth. For the isothermal study, as the crystallization was carried out under higher temperatures, the polymeric segments were flexible and could be easily transport to the growing crystal surface. Hence, crystallization took place by a nucleation-controlled mechanism, and ϕ was mostly dominated by the process of nucleation. Because of the nucleating effect of POSS, the isothermal crystallization of the nanocomposites was thus accelerated.[29] However, for the nonisothermal crystallization procedure, the crystallization was carried out at lower temperatures. The crystal growth dominated ϕ in this situation.[30] The presence of POSS hindered the crystal growth, with the effect being more significant when more POSS was incorporated. This resulted in a decrease in ϕ.

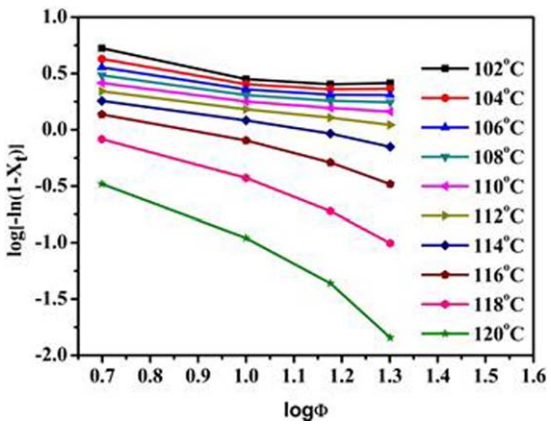

Figure 8. Ozawa plots for the nonisothermal crystallization of UHMWPE/POSS-0.0%. [Color figure can be viewed in the online issue, which is available at wileyonlinelibrary.com.]

The activation energy (ΔE) for the transport of the macromolecular segments to the growing crystal surface were evaluated from the Kissinger method:

Table IV. Values of B and $F(T)$ versus X_t

		X_t (%)			
		20	40	60	80
UHMWPE/POSS-0.0%	B	1.27	1.24	1.25	1.29
	$F(T)$	2.21	3.88	5.35	10.10
UHMWPE/POSS-1.0%	B	1.28	1.27	1.32	1.33
	$F(T)$	2.23	3.82	5.73	10.52
UHMWPE/POSS-1.5%	B	1.22	1.22	1.26	1.26
	$F(T)$	2.35	4.28	6.11	11.08
UHMWPE/POSS-2.3%	B	1.52	1.43	1.42	1.40
	$F(T)$	2.60	4.53	6.41	11.37

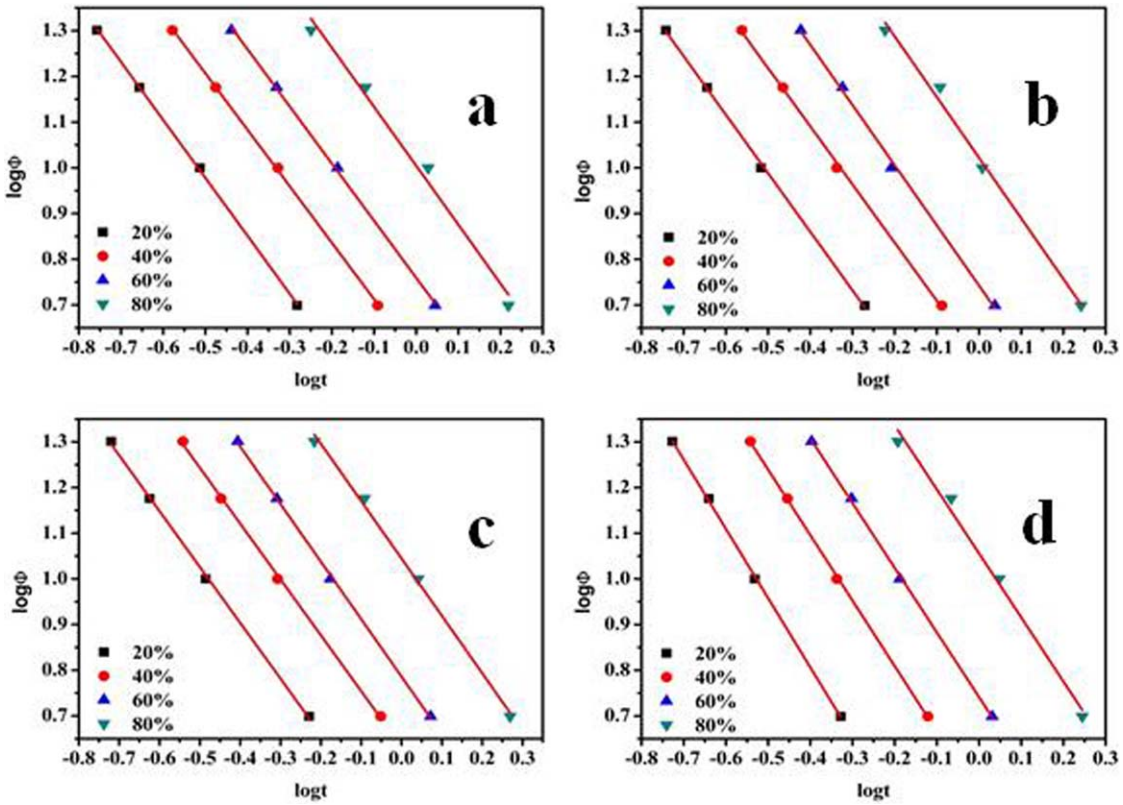

Figure 9. Plots of log Φ versus log t for (a) UHMWPE/POSS-0.0%, (b) UHMWPE/POSS-1.0%, (c) UHMWPE/POSS-1.5%, and (d) UHMWPE/POSS-2.3%. [Color figure can be viewed in the online issue, which is available at wileyonlinelibrary.com.]

$$\frac{d\left[\ln\left(\phi/T_p^2\right)\right]}{d\left(1/T_p\right)} = -\frac{\Delta E}{R} \tag{5}$$

where R is the universal gas constant. The plots of $\ln(\phi/T_p)$ versus $1/T_p$ based on the Kissinger method are shown in Figure 10. The slopes of the lines drawn through these plots were equal to $-\Delta E/R$, and thus, ΔE could be calculated. The results are summarized in Table V. It was shown that ΔE of the UHMWPE nanocomposites gradually decreased when the POSS concentration increased. This indicated that the nucleating effect of POSS was rather strong.[31]The OH-POSS used in this study had many hydroxyl groups. It enhanced the interaction with the UHMWPE segments through the hydrogen bonds.[11,21] This may be the reason that OH-POSS served as the nucleating agent in the UHMWPE/POSS nanocomposites.

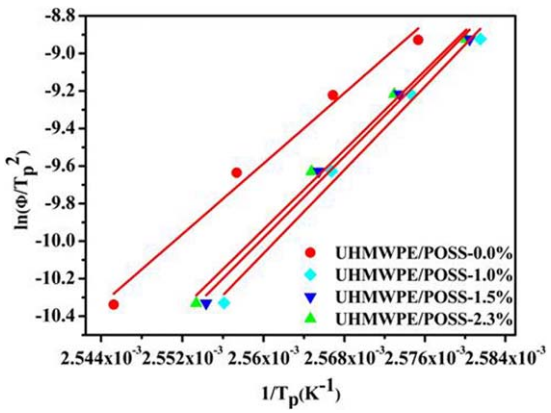

Figure 10. Kissinger plots of the UHMWPE/POSS nanocomposites. [Color figure can be viewed in the online issue, which is available at wileyonlinelibrary.com.]

CONCLUSIONS

In this study, UHMWPE/OH-POSS nanocomposites were synthesized according to an ethylene *in situ* polymerization procedure. The POSS with strong polarity dispersed in the UHMWPE matrix on a nanosize scale. The influence of the POSS concentration on the isothermal and nonisothermal crystallization kinetics of UHMWPE was studied with the DSC method. The isothermal studies showed that the crystallization rate constant was affected by the concentration of POSS, as we observed a pronounced increase with increasing POSS content. It was possible that POSS acted as a nucleus for the initial nucleation and subsequent growth of the crystallites. For

Table V. ΔE Values of the UHMWPE/POSS Nanocomposites as Determined on the Basis of the Kissinger Method

Entry	$-\Delta E$ (kJ/mol)
UHMWPE/POSS-0.0%	450.4
UHMWPE/POSS-1.0%	450.6
UHMWPE/POSS1.5%	439.9
UHMWPE/POSS-2.3%	390.6

nonisothermal studies, POSS showed an increase in the crystallinity of the nanocomposites. However, the ϕ values of the nanocomposites decreased because the presence of POSS hindered the crystal growth. The effect was more significant when more POSS was incorporated. ΔE for the transport of the macromolecular segments to the growing crystal surface gradually decreased when the POSS concentration increased. This indicated that the nucleating effect of POSS was rather strong.

ACKNOWLEDGMENTS

Funding from the Project of the Natural Science Foundation of China (contract grant number 21206078), the Natural Science Foundation of Zhejiang Province (contract grant number LQ12B06003), the Natural Science Foundation of Ningbo (contract grant number 2013A610026), the Zhejiang Province Department of Education Fund (contract grant number Y201223797), the Key Innovation Team of Zhejiang Province (contract grant number 2011R50001), and the Magna Fund of Ningbo University (sponsored by K. C. Wong) is gratefully acknowledged.

REFERENCES

1. Sharma, K. G. Ph.D. Thesis, Eindhoven University of Technology, 2005.
2. Green, M. S.; Tobolsky, A. V. *J. Chem. Phys.* **1946**, *14*, 80.
3. Lodge, A. S. *Trans. Faraday Soc.* **1956**, *52*, 120.
4. Yamamoto, M. *J. Phys. Soc.* **1956**, *11*, 413.
5. Pavlidou, S.; Papaspyrides, C. D. *Prog. Polym. Sci.* **2008**, *33*, 1119.
6. He, F. A.; Zhang, L. M. *Nanotechnology* **2006**, *17*, 5941.
7. Fang, L.; Leng, Y.; Gao, P. *Biomaterials* **2006**, *27*, 3701.
8. Zhang, Q. H.; Lippits, D. R.; Rastogi, S. *Macromolecules* **2006**, *39*, 658.
9. Paul, D. R.; Robeson, L. M. *Polymer* **2008**, *49*, 3187.
10. Kawasumi, M. *J. Polym. Sci. Part A: Polym. Chem.* **2004**, *42*, 819.
11. Li, W.; Adams, A.; Wang, J. D.; Blümich, B.; Yang, Y. R. *Polymer* **2010**, *51*, 4686.
12. Gopakumar, T. G.; Lee, J. A.; Kontopoulou, M.; Parent, J. S. *Polymer* **2001**, *43*, 5483.
13. Ahangari, M. G.; Fereidoon, A.; Kordani, N.; Garmabi, H. *Polym. Bull.* **2011**, *66*, 239.
14. Shi, X. M.; Wang, J. D.; Jiang, B. B.; Yang, Y. R. *J. Appl. Polym. Sci.* **2013**, *128*, 3609.
15. Mitani, M.; Mohri, J.; Yoshida, Y.; Saito, J. J.; Ishi, S.; Tsuru, K.; Matsui, S.; Furuyama, R.; Nakano, T.; Tanaka, H.; Kojoh, S.; Matsugi, T.; Kashiwa, N.; Fujita, T. *J. Am. Chem. Soc.* **2002**, *124*, 3327.
16. Makio, H.; Kashiwa, N.; Fujita, T. *Adv. Synth. Catal.* **2002**, *344*, 477.
17. Rastogi, S.; Kurelec, L. *J. Mater. Sci.* **2000**, *35*, 5121.
18. Ye, Z. B.; Alsyourib, H.; Zhu, S. P.; Lin, Y. S. *Polymer* **2003**, *44*, 969.
19. Zhou, Q.; Wang, Z.; Shi, Y.; Fang, J.; Gao, H.; Loo, L. S. *Appl. Surf. Sci.* **2013**, *284*, 118.
20. Gopakumar, T. G.; Lee, J. A.; Kontopoulou, M.; Parent, J. S. *Polymer* **2003**, *43*, 5483.
21. Misra, R.; Alidedeoglu, A. H.; Jarrett, W. L.; Morgan, S. E. *Polymer* **2009**, *50*, 2906.
22. Zhou, Q.; Pramoda, K. P.; Lee, J. M.; Wang, K.; Loo, L. S. *J. Colloid Interface Sci.* **2011**, *335*, 222.
23. Avrami, M. *J. Chem. Phys.* **1939**, *7*, 1103.
24. Avrami, M. *J. Chem. Phys.* **1941**, *9*, 177.
25. Tobin, M. C. *J. Polym. Sci. Polym. Phys. Ed.* **1974**, *12*, 399.
26. Long, Y.; Shanks, R. A.; Stachursk, Z. H. *Prog. Polym. Sci.* **1995**, *20*, 651.
27. Huang, J. W. *J. Appl. Polym. Sci.* **2008**, *107*, 3163.
28. Adhikari, A. R.; Lozano, K.; Chipara, M. *J. Compos. Mater.* **2012**, *46*, 823.
29. Joshi, A.; Butola, B. S. *Polymer* **2004**, *45*, 4953.
30. Yuan, Q.; Awate, S.; Misra, R. D. K. *J. Appl. Polym. Sci.* **2006**, *102*, 3809.
31. Gopakumar, T. G.; Lee, J. A.; Kontopoulou, M.; Parent, J. S. *Polymer* **2002**, *43*, 5483.